International Journal for Housing Science and Its Applications
Publish August 6, 2025. Volume 46, Issue 3 Pages 4965-4973

https://doi.org/10.70517/ijhsa463425

Fatigue Threshold and Crack Expansion Behavior of Natural Gas Pressure Vessel Steels and Yield Strength Dependence Analysis Based on Multiscale Modeling Approach

Gao Zhang[1,*], Yajuan Wang[2], Junpeng Kang[1] and Jia Li[3]
[1] School of Architectural Surveying and Mapping, Shaanxi Energy Institute, Xianyang, Shaanxi, 712000, China
[2] School of Intelligent Mechatronics, Shaanxi Energy Institute, Xianyang, Shaanxi, 712000, China
[3] School of Construction Machinery, Chang'an University, Xi'an, Shaanxi, 710064, China
Corresponding authors: (e-mail: sanhu1989hugh@163.com).

Abstract As a key pressure-bearing equipment, the degree of fatigue failure of natural gas pressure vessel affects the operational safety. Based on finite element stress analysis and Kwofie-Zhu model, this paper establishes an equivalent driving force model considering crack closure effect. Combined with the Johnson-Cook thermo-viscoplastic constitutive equation and the fluid-solid coupling algorithm, the numerical analysis model of explosion crack extension is constructed. The correlation of stress ratio (R) to fatigue threshold (ΔKth) and the effect of yield strength on crack extension rate are revealed through multi-scale modeling analysis. The results showed that ΔKth decreased from 7.32MPa·m1/2 to 5.45MPa·m1/2 when R was increased from 0.05 to 0.35. The crack extension rate increased from 10-9cm/s to 10-8cm/s when the yield strength was increased from 282 MPa to 582 MPa. The multiscale modeling analysis reveals that R has a negative correlation with ΔKth, and the yield strength varies positively with the crack extension rate.

Index Terms finite element analysis, Kwofie-Zhu model, intrinsic model, fluid-solid coupling, fatigue threshold value

I. Introduction

Natural gas pressure vessels are mainly used for storing and transporting natural gas, and their safe operation is directly related to the normal operation and safe production of natural gas stations [1], [2]. The importance of natural gas pressure vessels is not only reflected in its importance to the operation of natural gas stations, but also in its importance to the society and the environment [3], [4]. Once an accident such as leakage or explosion occurs in a natural gas pressure vessel, it will cause serious threats to the surrounding environment and people's lives and properties [5]. Therefore, it is important to study the fatigue threshold value of natural gas pressure vessel steel with crack extension behavior and yield strength dependence to ensure the safe operation of natural gas stations, safeguard people's lives and properties, and protect the safety of the environment [6]-[8].

Fatigue crack threshold, is the stress level at which cracks begin to expand under material fatigue loading [9]. Under material fatigue loading, when the stress is less than the fatigue cracking threshold, the crack will not expand, while when the stress exceeds the threshold, the crack will begin to expand [10]-[12]. The size of the fatigue cracking threshold depends on factors such as the nature of the material, microstructure, surface quality and loading conditions [13], [14]. Yield strength is the maximum value of stress that a material can withstand when subjected to sustained loading, beyond which the material will deform plastically [15]. Yield strength is an important parameter for materials under loading conditions such as tension, compression or bending and is commonly used to assess the strength and toughness of materials [16]-[18]. From the perspective of materials science, both fatigue crack threshold and yield strength are important mechanical property parameters of materials [19]. The fatigue crack threshold reflects the crack extension resistance of a material under fatigue loading, while the yield strength reflects the deformation resistance of a material under sustained loading [20], [21]. These two parameters are important for engineering design and material selection.

In this paper, starting from the finite element stress analysis, the three-dimensional solid model of steel CNG bottle is established, and the mesh division and boundary setting are completed by combining the symmetric constraints and loading conditions. The Kwofie-Zhu model is constructed, and the crack closure coefficient is introduced to correct the stress intensity factor range, and the influence of the closure effect on the fatigue threshold is analyzed. For the dynamic crack extension problem, the Johnson-Cook intrinsic model is used to describe the strain rate effect of the material, and the correlation between crack extension and fluid dynamic response is analyzed by combining the ALE fluid-solid coupling algorithm and the cell deletion technique.

II. Analysis of research methods

This chapter describes the techniques related to the study of the relationship between fatigue threshold and crack extension behavior and yield strength dependence of natural gas pressure vessel steels through modeling analysis.

II. A.Finite element stress analysis

II. A. 1) Analysis objects and calculation models

The existing steel CNG bottle pressure vessel has an outer diameter of D=561mm, a wall thickness of 31mm, and a working pressure of 31MPa. It is made of high-pressure seamless steel pipe, and its material properties are: E=2.1104MPa, μ=0.32, and the yield limit σy=482MPa.

Calculation model selection: the steel CNG bottle pressure vessel is a slender cylinder pressure vessel with inlet and outlet at both ends, taking a certain length of the cylinder (402mm) and the end as the object of calculation, and at the same time, due to the symmetry of the structure, half of it is taken for modeling. The calculation unit type is 8-node 3D solid unit (SOLID45); the boundary conditions are: symmetry constraints are applied on the symmetry plane, and the truncation plane is fixed by hinged support; the loads are: 31MPa internal pressure and 16.873MPa axial stress on the inlet/outlet section.

II. A. 2) Finite element meshing

Now the finite element analysis is carried out for the steel CNG bottle pressure vessel with outer diameter D of 561mm, wall thickness of 31mm, caliber d of 91mm, and transition arc radius R of 141mm.

The mesh is mapped and divided into five layers along the thickness of the steel CNG bottle pressure vessel, and the whole computational model is divided into 23,202 cells and 28,906 nodes.

II. B.Kwofie-Zhu modeling

The Kwofie-Zhu model is based on an equivalent driving force model while considering the contribution of crack closure. The equivalent driving force model is shown in equation (1).

$$\Delta K_{eq} = \Delta K_R \exp\left(\alpha\left(\frac{1+R}{1-R}\right)\right) \tag{1}$$

where ΔK_{eq} is the range of equivalent stress intensity factors and ΔK_R is the range of stress intensity factors at any R. The condition for Eq. (1) to hold is that the stress intensity factor ranges corresponding to da/dN on both sides of the equation are the same, and it is suitable for characterizing the fatigue crack extension behaviors of different R at higher da/dN.

By introducing the K_{op} parameter to represent the crack tensile stress intensity factor, the crack closure effect is thus included in the model. For $\Delta K = K_{\max} - K_{\min}$, when there is crack closure, $K_{\min} < K_{op}$, in this case, ΔK should be taken as the effective portion of the crack closure stress factor, which is denoted by ΔK_{eff}, i.e. $\Delta K_{eff} = K_{\max} - K_{op}$. For this reason equation (1) can be rewritten as

$$\Delta K_{eq} = \Delta K_{eff} \exp\left(\alpha\left(\frac{1+R}{1-R}\right)\right) \tag{2}$$

where ΔK_{eff} can be written in the form

$$\Delta K_{eff} = \begin{cases} K_{\max} - K_{op} & K_{\min} < K_{op} \\ K_{\max} - K_{\min} & K_{\min} \geq K_{op} \end{cases} \tag{3}$$

A further transformation of equation (3)

$$\Delta K_{eff} = \begin{cases} K_{\max}\left(1 - \dfrac{K_{op}}{K_{\max}}\right) & \dfrac{K_{\min}}{K_{\max}} < \dfrac{K_{op}}{K_{\max}} \\ K_{\max}\left(1 - \dfrac{K_{\min}}{K_{\max}}\right) & \dfrac{K_{\min}}{K_{\max}} \geq \dfrac{K_{op}}{K_{\max}} \end{cases} \tag{4}$$

Knowing that $R = K_{\min}/K_{\max}$ and letting $R_c = K_{op}/K_{\max}$, equation (4) can be rewritten as

$$\Delta K_{eff} = \begin{cases} K_{\max}(1-R_c) & R < R_c \\ K_{\max}(1-R) & R \geq R_c \end{cases} \tag{5}$$

where R_c is called the critical stress ratio or transition stress ratio, and its physical significance is that when $R \geq R_c$, there is no crack closure at any given da/dN, and it is clear that the lower the da/dN, the corresponding K_{op} is higher, when da/dN is sufficiently small or close to the threshold at $(da/dN)_{th}$, the value of $K_{op}/K_{\max}$ can be taken as the value of R_c. At this point, Eq. (5) can be further transformed

$$\Delta K_{eff} = \begin{cases} \Delta K_R \left(\dfrac{1-R_c}{1-R}\right) & R < R_c \\ \Delta K_R & R \geq R_c \end{cases} \tag{6}$$

Thus, Eq. (1) can eventually be changed to

$$\Delta K_{eq} = \begin{cases} \Delta K_R \left(\dfrac{1-R_c}{1-R}\right) \exp\left(\alpha\left(\dfrac{1+R}{1-R}\right)\right) & R < R_c \\ \Delta K_R \exp\left(\alpha\left(\dfrac{1+R}{1-R}\right)\right) & R \geq R_c \end{cases} \tag{7}$$

Here, defining the crack closure factor $U(R) = \Delta K_{eff}/\Delta K_R$, we get from equation (5)

$$\Delta K_{eq} = \Delta K_R U(R) \exp\left(\alpha\left(\frac{1+R}{1-R}\right)\right) \tag{8}$$

If we introduce the function $f(R)$ again, let

$$f(R) = U(R)\exp\left(\alpha\left(\frac{1+R}{1-R}\right)\right) = \begin{cases} \left(\dfrac{1-R_c}{1-R}\right)\exp\left(\alpha\left(\dfrac{1+R}{1-R}\right)\right) & R < R_c \\ \exp\left(\alpha\left(\dfrac{1+R}{1-R}\right)\right) & R \geq R_c \end{cases} \tag{9}$$

Then equation (8) further simplifies to

$$\Delta K_{eq} = \Delta K_R f(R) \tag{10}$$

Due to the arbitrariness of R, equation (10) can also be written as

$$\Delta K_{R_{ef}} f(R_{ef}) = \Delta K_R f(R) \tag{11}$$

Or:

$$\Delta K_R = \Delta K_{R_{er}} \frac{f(R_{ef})}{f(R)} \tag{12}$$

where R_{ef} represents the known reference stress ratio. If $R_{ef} = 0.1$ is taken, then from Eq. (12) we have

$$\frac{\Delta K_R}{\Delta K_{0.1}} = \frac{f(0.1)}{f(R)} = \begin{cases} \left(\dfrac{1-R}{1-0.1}\right)\exp\left(\alpha\left(\dfrac{11}{9}-\dfrac{1+R}{1-R}\right)\right) & R < R_c \\ \left(\dfrac{1-R_c}{1-0.1}\right)\exp\left(\alpha\left(\dfrac{11}{9}-\dfrac{1+R}{1-R}\right)\right) & R \geq R_c \end{cases} \tag{13}$$

Eq. (13) represents the ΔK relationship between different R under the same da/dN, and accordingly, there is a correlation between different R under the same $\Delta K_{R_{ef}}$ between da/dN. According to equation (12), da/dN is modeled as

$$\left(\frac{da}{dN}\right)_{R_{er}} = C(\Delta K_R)^m \left(\frac{f(R)}{f(R_{ef})}\right)^n \tag{14}$$

where $n \neq m$. Then we have

$$\left(\frac{da}{dN}\right)_{R_{er}} = \left(\frac{da}{dN}\right)_R \left(\frac{f(R)}{f(R_{ef})}\right)^n \tag{15}$$

Eq. (15) holds if both sides of the equation da/dN correspond to the same $\Delta K_{R_{ef}}$.

II. C.Natural gas pressure vessel explosion fluid-solid coupling numerical analysis modeling

II. C. 1) Intrinsic Modeling and Failure Criteria

As the crack extension rate can be as high as $10^3 \mathrm{m/s}$ during the physical explosion of gas storage cylinders, the material in front of the crack tip is loaded with a high strain rate, and the mechanical properties of the material are affected by the joint influence of strain hardening, strain rate hardening and temperature softening effects. Based on this, this paper adopts the thermo-viscoplastic model Johnson-Cook (J-C) intrinsic model to describe the stress-strain relationship of the bottle material:

$$\sigma = \left(A + B\bar{\varepsilon}^n\right)\left(1 + C\ln\dot{\bar{\varepsilon}}^*\right)\left[1 - \left(\frac{T - T_r}{T_m - T_r}\right)^m\right] \tag{16}$$

where σ is the material equivalent stress, MPa; $\bar{\varepsilon}$ is the material equivalent plastic strain; $\dot{\bar{\varepsilon}}^*$ is the dimensionless equivalent plastic strain rate; $\dot{\varepsilon}_0$ is the reference strain rate; T_r and T_m are the reference and melting temperatures of the material, K respectively. The three terms from left to right of the $J-C$ model characterize the strain hardening, strain rate hardening, and temperature softening of the material, respectively, and A, B, C, n, and m are the material's parameters to be determined.

The simulation of the crack extension process is realized by the unit deletion (ED) method combined with the $J-C$ failure criterion, and the failure strain is defined in the $J-C$ failure criterion as:

$$\varepsilon^f = \left[D_1 + D_2 \exp D_3\sigma^*\right]\left[1 + D_4 \ln\dot{\varepsilon}^*\right]\left[1 + D_5\left(\frac{T - T_r}{T_m - T_r}\right)\right] \tag{17}$$

where ε^f is the failure strain; σ^* is the dimensionless stress ratio; D_1, D_2, D_3, D_4, D_5 are the parameters to be determined.

Among them, in the process of physical explosion crack extension, the temperature difference between the front and rear of the storage cylinder is small, and the change of material properties caused by the temperature is low, so this paper does not consider the change of mechanical properties of the material caused by the temperature, and will be $D_5 = 0$.

II. C. 2) Gas Equation of State

In this paper, both the high-pressure natural gas inside the bottle and the outside air are described by the inviscid ideal gas equation, and the high-pressure natural gas leakage is assumed to be an isentropic adiabatic process.

$$P = (\gamma - 1)\rho e \tag{18}$$

where P is the pressure at the fixed point, Pa; γ is the adiabatic index of the gas; ρ is the mass density of the gas, $\mathrm{kg/m^3}$; and e is the energy density at the fixed point, J/kg.

For the simulations in this paper, the initial air density ρ_{Air} and natural gas density $\rho_{\mathrm{Natural\ gas}}$ are $1.28\mathrm{kg/m^3}$ and $0.718\mathrm{kg/m^3}$, respectively, and the air adiabatic index γ_{Air} and natural gas adiabatic index $\gamma_{\mathrm{Natural\ gas}}$ are 1.41 and 1.315, respectively.

II. C. 3) Flow-solid coupling algorithm

The physical explosion crack extension of gas cylinder is a kind of fluid-solid coupling accompanied by extreme deformation and fracture, in order to solve the problem, this paper adopts the ALE algorithm to realize the coupling

of fluid (natural gas, air) and structure (gas cylinder), and the penalty function method is used to calculate the contact force between the fluid and the solid, which is directly proportional to the contact stiffness and the contact depth. Due to the large difference in density and stiffness between the fluid material and the structure material, coupling simulation will often appear penetration, leakage, computational instability and other problems, so this paper comprehensively consider the computational stability, the overall time step and the node mass to get the size of the contact stiffness:

$$k = \max\left(\frac{Ks^2}{v}, \frac{m}{\Delta t^2}\right) \tag{19}$$

where K is the bulk modulus of the material; s is the contact area; v is the unit volume; m and Δt are the nodal mass and time step, respectively.

At present, there is a lack of experiments related to the physical explosion crack extension of gas storage cylinders, which makes it difficult to be verified directly by simulation. However, the thermo-viscoplastic constitutive model and the fluid-solid coupling algorithm used in this paper have been used in the simulation of pipeline crack extension under explosion load, and verified with experiments, which illustrates the accuracy of the relevant models and algorithms.

III. Analysis of fatigue threshold correlation law based on multi-scale modeling

In this chapter, the constructed model is used to analyze the fatigue threshold value of natural gas pressure vessel steel in relation to the crack extension behavior and yield strength dependence, and to excavate the laws that exist in it.

III. A. Analysis of fracture location and its relation to stress intensity

III. A. 1) Fracture location statistics

The fracture locations of the fatigue specimens of steel CNG cylinders were analyzed. Figure 1 shows the distribution of the fracture locations, and the solid line at 108 represents the change of the cracks from surface initiation to internal initiation. Most of the specimens close to the solid line at 108 fracture in the weld area, which shows that the long-life specimens tend to fatigue fracture at the weld. The fracture locations of the specimens at all lifetimes were counted. Although the long-life specimens fractured at the weld seam, the number of specimens that fractured at the base material was higher than that of the weld seam at the full-life stage, and it can be seen that at the short-life stage, more specimens fractured at the base material, and the number of specimens that fractured at the heat-affected zone was the lowest.

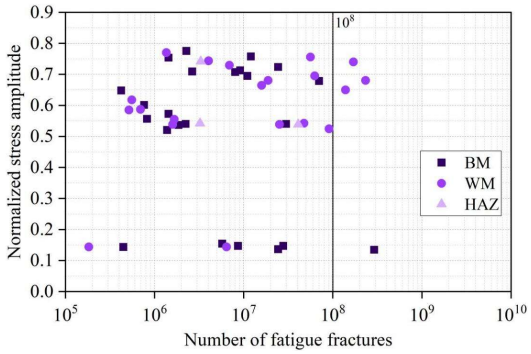

Figure 1: Fracture location distribution

III. A. 2) Relationship between the number of faceted fracture surfaces and the stress intensity factor

The number of face-type fracture surfaces reflects the strength of the crack closure effect induced by roughness, which has a direct influence on the fatigue threshold, so it is necessary to study the number of face-type fracture surfaces in depth. From the micropatterns, it is seen that the number of face-type fracture surfaces varies with ΔK during fatigue crack extension, while the number of face-type fracture varies with different R or different heat treatment conditions.

The percentage of facet fracture was obtained by measuring the area of facet fracture in the SEM images of the section using image processing software, and at least five points were counted for each ΔK, and the average value was taken as the percentage of facet fracture at that ΔK. Fig. 2 demonstrates the relationship between the

percentage of facet fracture and ΔK. The facet fracture has a parabolic distribution and reaches the maximum value at a certain ΔK; the maximum facet fracture fractions corresponding to ΔK for the two heat treatment conditions, 500°C*24h and 600°C*24h, are close to each other with an error of no more than 3MPa·m1/2 when R is 0.15 and 0.75, and the maximum facet fracture fractions corresponding to the two heat treatment conditions, 500°C*24h and 600°C*24h, are close to each other with an error of no more than 3 MPa-m1/2; whereas, when R is 0.35, there is a large deviation in ΔK for the maximum value of face fracture. It can be inferred that the reason for the difference in fatigue thresholds at R of 0.35 is related to the change in the crack extension mechanism in the near-threshold region, where the percentage of fracture face-type fracture gradually decreases with increasing R.

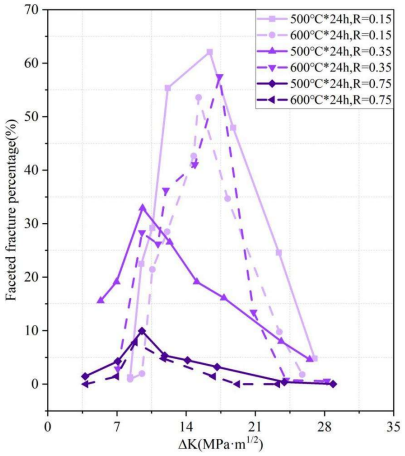

Figure 2: The relation between percentage of facet fracture and ΔK

III. B. Fatigue crack extension law analysis

III. B. 1) Determination of Fatigue Crack Expansion Thresholds

The fatigue crack extension threshold is the range of stress intensity factors at the crack tip that corresponds to the cessation of fatigue crack extension in a fatigue test. In fact, it is impossible to stop crack expansion “absolutely”, so the stress intensity factor range ΔK at da/dN=10-7mm/cycle is defined as the fatigue crack expansion threshold ΔKth (a is the crack length, N is the number of cycles). The model of this paper was utilized to obtain five points with crack extension rates in the interval from 10-10mm/cycle to 10-9mm/cycle. These 5 data points were then fitted with a straight line in the da/dN-ΔK double logarithmic coordinate system. Finally, the ΔK value obtained by substituting da/dN=10-10mm/cycle into the equation of the straight line obtained from the fit is ΔKth. Note that when there are less than 5 points in the interval, a point with a da/dN slightly greater than 10-9mm/cycle can be used for the fit. The graded load reduction is controlled at 10% per stage, and the crack extension increment Δa is to be greater than 5-7 times the plastic zone size ry corresponding to the Kmax of the previous stage at each level of force. Figure 3 shows the obtained test data and their fitted straight lines in double logarithmic coordinates. The fatigue crack thresholds are 7.32, 6.99, 6.42, and 5.45MPa·m1/2 for stress ratios R equal to 0.05, 0.15, 0.25, and 0.35, respectively, and the fatigue crack thresholds ΔKth decrease with the increase of stress ratio.

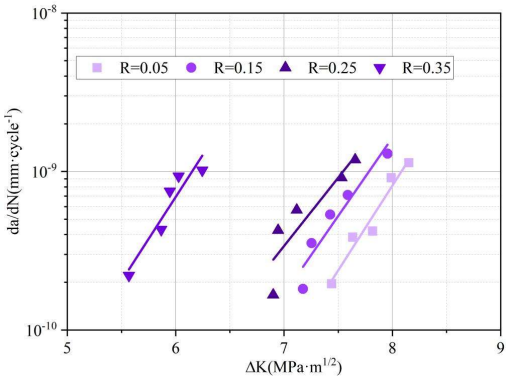

Figure 3: Test results of fatigue crack threshold values

III. B. 2) Fatigue crack extension rate

The average stress level of the fatigue cycle has a great influence on the fatigue behavior of CNG bottle materials, and the stress ratio R is commonly used to describe the average stress. Fig. 4 shows the fatigue crack expansion rate of the specimen at different stress ratios R where ΔP is the range of force values, i.e., ΔP=Pmax-Pmin, and is the difference between the maximum and minimum values of the alternating load. From Fig. 4, it can be seen that as the stress ratio gradually increases from 0.05 to 0.35, the crack extension rate corresponding to the same stress intensity factor range of ΔK values increases subsequently. It shows that the crack extension behavior exhibits a relatively obvious stress ratio effect. Further observation reveals that the difference between the crack extension rates due to stress ratios is evident at smaller values of ΔK (30MPa·m1/2). With the further increase of ΔK value, the difference between the crack extension rates at each stress ratio has a tendency to decrease.

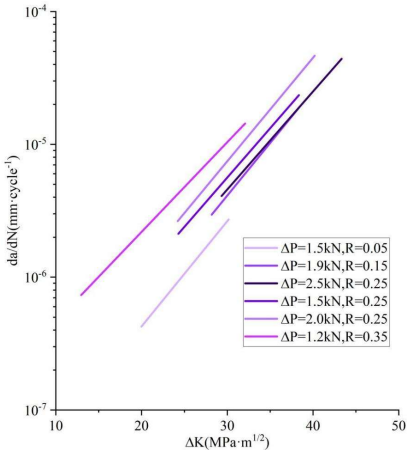

Figure 4: Fatigue crack growth rates under different stress ratios R

III. C. Effect of yield strength on crack extension rate

Fig. 5 shows the effect of yield strength on crack extension rate at different stress intensity factors predicted by the principal model. From the figure, it can be seen that there is an increase in the crack extension rate as the yield strength increases from 282 MPa to 582 MPa at the same stress intensity factor. For example, the crack extension rate increases from 10-9cm/s to 10-8cm/s with the increase of yield strength at 110MPa·m1/2 stress intensity factor. However, in combination with the predictions of other models, it can be found that the change in crack extension rate due to the change in yield strength in the crack tip strain rate equation used in the present model does not fully explain the phenomenon of change in crack extension rate of CNG bottles due to the change in yield strength. In other words, the effect of yield strength on crack extension rate predicted by the constitutive model is smaller than that predicted by other models. This is because only the effect of yield strength on crack tip strain rate is taken into account in the present constitutive model, but not the changes in the process of yield strength variation such as the degree of cold working, grain size, deposition distribution and strain intensification factor. Therefore, in order to improve the ability of the constitutive model to predict the effect of yield strength on the crack extension rate, a corresponding correction factor needs to be introduced.

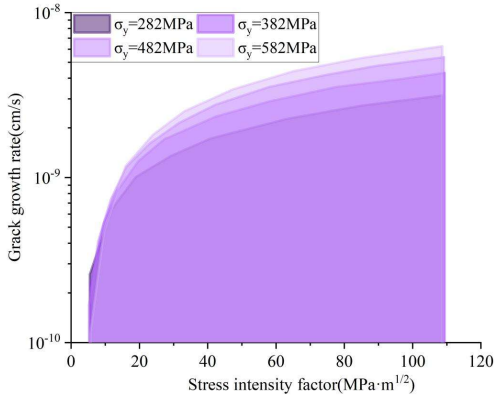

Figure 5: Effect of yield strength on CGR using J-C model

Fig. 6 shows the relationship between the crack extension rate and the stress intensity factor predicted by the intrinsic model at yield strengths of 395 MPa and 469 MPa, respectively. When the stress intensity factor is below 35MPa·m1/2, the crack extension rate increases rapidly from about 10-12cm/s to about 10-8cm/s with the increase of the stress intensity, which can be seen that the stress intensity plays a decisive role in the crack extension rate at this time, and the crack extension rate is mainly controlled by the stress intensity. However, when the stress intensity is greater than 35MPa·m1/2, the growth rate of crack extension rate with the change of stress intensity becomes slower, and the influence of mechanical factors (stress intensity) on the crack extension rate decreases, at this time, the nature of the material (e.g., yield strength) or the environmental factors (e.g., pH, ECP) begin to play a decisive role. From Fig. 6, it can be seen that the yield strength of the material has an important effect on the crack extension rate, and when the environmental factors and stress intensity are the same, the corresponding crack extension rate increases when the yield strength of the material is increased, and this result is also consistent with the results predicted by other models.

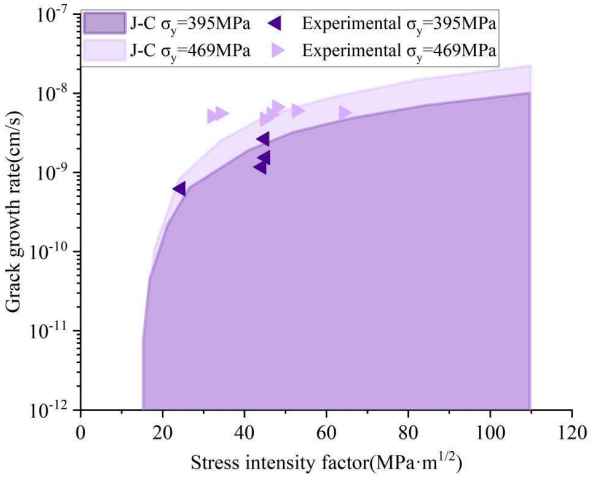

Figure 6: Prediction of crack growth rate vs. KI using J-C model

IV. Conclusion

In this paper, the correlation law between fatigue threshold value and crack extension behavior and yield strength of natural gas pressure vessel steel is systematically analyzed through multi-scale modeling and numerical simulation. The fatigue threshold value decreases significantly with the increase of the stress ratio, and the maximum fatigue threshold value reaches 7.32MPa·m1/2 when the stress ratio is 0.05 at the minimum. The fatigue threshold decreases to 5.45MPa·m1/2 when the stress ratio reaches 0.35. The crack extension rate is dominated by the stress ratio in the low stress intensity region, while it is more significantly affected by the yield strength of the material in the high stress intensity region. The crack extension rate is enhanced by nearly an order of magnitude when the yield strength is increased from 282 MPa to 582 MPa. Future studies can introduce microstructural parameters for continuous optimization of the model to improve the analytical effectiveness of the model.

Funding

This work was supported by Scientific Research Program Funded by Education Department of Shaanxi Provincial Government (Program No. 22JK0326) and Shaanxi Province's Key Research and Development Program (General Projects) (Program No. 2024GX-YBXM-253) and School-level Research Projects of Shaanxi Energy Institute of Technology (Program No. 2021QN04).

References

[1] Jegatheesan, J., & Zakaria, Z. (2018). Stress analysis on pressure vessel. Environ. Ecosyst. Sci, 2, 53-57.

[2] Kwak, H. S., Park, G. Y., & Kim, C. (2020). Design of compressed natural gas pressure vessel (Type II) to improve storage efficiency and structural reliability. Journal of Pressure Vessel Technology, 142(1), 011303.

[3] Kim, Y. S., Kim, L. H., & Park, J. S. (2011). The effect of composite damage on fatigue life of the high pressure vessel for natural gas vehicles. Composite Structures, 93(11), 2963-2968.

[4] Liao, K., Qin, M., He, G., Chen, S., Jiang, X., & Zhang, S. (2023). Improvement of integrity management for pressure vessels based on risk assessment-A natural gas separator case study. Journal of Loss Prevention in the Process Industries, 83, 105087.

[5] Yersak, T. A., Abd Elhamid, M., Dailly, A., Rogers, M., Prince, J., & Cai, M. (2019). Dynamics of a type IV conformable pressure vessel for natural gas passenger vehicles. International Journal of Pressure Vessels and Piping, 175, 103923.

[6] Zhang, G., Wang, Y., Kang, J., & Li, J. (2025). Calculation of Fatigue Threshold and Crack Expansion Rate of Natural Gas Pressure Vessel Steels and Yield Strength Dependence Analysis. J. COMBIN. MATH. COMBIN. COMPUT, 127, 7721-7746.
[7] Lee, S. M., Park, S. Y., Baek, U. B., & Choi, B. H. (2023). Evaluation of the residual fatigue lifetime of a semi-elliptical crack of a Low-Alloy steel pressure vessel under High-Pressure gaseous hydrogen. International Journal of Fatigue, 176, 107875.
[8] Slifka, A. J., Drexler, E. S., Amaro, R. L., Hayden, L. E., Stalheim, D. G., Lauria, D. S., & Hrabe, N. W. (2018). Fatigue measurement of pipeline steels for the application of transporting gaseous hydrogen. Journal of Pressure Vessel Technology, 140(1), 011407.
[9] Sadananda, K., Babu, M. N., & Vasudevan, A. K. (2019). A review of fatigue crack growth resistance in the short crack growth regime. Materials Science and Engineering: A, 754, 674-701.
[10] Peixoto, D. F., & de Castro, P. M. (2017). Fatigue crack growth of a railway wheel. Engineering failure analysis, 82, 420-434.
[11] Thurston, K. V., Gludovatz, B., Hohenwarter, A., Laplanche, G., George, E. P., & Ritchie, R. O. (2017). Effect of temperature on the fatigue-crack growth behavior of the high-entropy alloy CrMnFeCoNi. Intermetallics, 88, 65-72.
[12] Simoes, M., Braithwaite, C., Makaya, A., & Martínez‐Pañeda, E. (2022). Modelling fatigue crack growth in shape memory alloys. Fatigue & Fracture of Engineering Materials & Structures, 45(4), 1243-1257.
[13] Duarte, L., Schoenherr, J. A., Madia, M., Zerbst, U., Geilen, M. B., Klein, M., & Oechsner, M. (2022). Recent developments in the determination of fatigue crack propagation thresholds. International Journal of Fatigue, 164, 107131.
[14] Cai, X., Xia, R., Huo, M., & Xu, J. (2018). A threshold formula for fatigue crack growth with mean stress intensity factors. International Journal of Mechanical Sciences, 135, 639-645.
[15] Valíček, J., Harničárová, M., Kopal, I., Palková, Z., Kušnerová, M., Panda, A., & Šepelák, V. (2017). Identification of upper and lower level yield strength in materials. Materials, 10(9), 982.
[16] Li, W., Zhang, X., Kou, H., Wang, R., & Fang, D. (2016). Theoretical prediction of temperature dependent yield strength for metallic materials. International Journal of Mechanical Sciences, 105, 273-278.
[17] Armstrong, R. W. (2019). Size effects on material yield strength/deformation/fracturing properties. Journal of Materials Research, 34(13), 2161-2176.
[18] Lee, J. A., Figueiredo, R. B., Park, H., Kim, J. H., & Kim, H. S. (2024). Unveiling yield strength of metallic materials using physics-enhanced machine learning under diverse experimental conditions. Acta Materialia, 275, 120046.
[19] Li, C. L., Yuan, H., & Hong, H. P. (2023). Predicting yield strength of cold-formed carbon steel: A review and new approaches. Journal of Constructional Steel Research, 206, 107926.
[20] Madia, M., Vojtek, T., Duarte, L., Zerbst, U., Pokorný, P., Jambor, M., & Hutař, P. (2021). Determination of fatigue crack propagation thresholds for steel in presence of environmental effects. International Journal of Fatigue, 153, 106449.
[21] Yan, C., Liu, R., & Ou, Z. C. (2019). Analytical model for dynamic yield strength of metal. Physical Mesomechanics, 22, 333-339.